Anais IX Simpósio Brasileiro de Sensoriamento Remoto, Santos, Brasil, 11-18 setembro 1998, INPE, p. 1051-1061.

# Simultaneous generation and registration of SAR images

**David Fernandes**

Instituto Tecnológico de Aeronáutica (ITA)
Centro Técnico Aeroespacial (CTA)
Praça Mal. Eduardo Gomes, 50
12228-900 São José dos Campos, SP
david@ele.ita.cta.br

**Abstract**. Registration of SAR images is required for interferometric processing and multitemporal analysis. A procedure which allows simultaneous generation and registration of SAR images from spaceborne sensors is presented. The procedure is based on the properties of the chirp scaling algorithm and is used in a interferometric processor to generate the interferogram, the fringes and the coherence map.

**Keywords:** synthetic aperture radar, SAR image, registration of SAR images, SAR interferometry.

## 1 Introduction

To calculate the interferogram, the fringes and the coherence map of SAR images, the original Single-Look-Complex (SLC) SAR images must be registered. The miss registration decreases the correlation of the images and increases the phase error in the fringes of the interferogram.

The registration can be done after the generation of the SLC SAR images or it can be done simultaneously with the generation of the SLC images. This second approach results in a time reduction in the registration process, Fornaro et al. (1994), Fernandes et al. (1996).

In this work it is shown a process to simultaneously generate and register two SLC SAR images from spaceborne sensors and how this process can be used in a interferometric processor that can generate automatically the interferogram, the fringes and the coherence map.

## 2 SAR signal

A sample of a Real Aperture Radar (RAR) or a Synthetic Aperture Radar (SAR) image is generated by the backscattering of the transmitted signal within of a resolution cell. The dimension of a resolution cell is given by:

-for a RAR:

$$\text{in range} \qquad D_r = \frac{c_o T_p}{2} \quad [\text{m}] \tag{2.1}$$

$$\text{in azimuth} \qquad D_a = q_a \, r \quad [\text{m}] \tag{2.2}$$

$T_p$ is the transmitted signal pulsewidth, $c_o$ is the light speed, $q_a$ is the antenna beamwidth in azimuth and $r$ is the slant range between the radar antenna and the resolution cell center.

-for a SAR:

$$\text{in range} \qquad D_r = \frac{c_o}{2 \, B_r} \quad [\text{m}] \tag{2.3}$$

$$\text{in azimuth} \qquad D_a = \frac{v}{B_a} \quad [\text{m}] \tag{2.4}$$

$B_r$ is the transmitted chirp bandwidth given by $B_r = \gamma T_p$, where: $\gamma$ is the chirp rate, $v$ is the relative velocity between the scatter and the sensor platform, $B_a$ is the azimuth bandwidth given by: $B_a = g_a.T_a$, where $g_a$ is the azimuth chirp rate and $T_a$ is the illumination time:

$$g_a = \frac{2.v^2}{l.r} \quad [\text{Hz/s}] \tag{2.5}$$

$$T_a = \frac{r.q_a}{v} \quad [\text{s}] \tag{2.6}$$

$\lambda$ is the carrier frequency wavelength.

The pixel spacing gives the distance between two consecutive resolution cells. For the RAR or SAR systems it is given by:

$$\text{in range} \qquad d_r = \frac{c_o T_s}{2} \quad [\text{m}] \tag{2.7}$$

$$\text{in azimuth} \qquad d_a = \frac{v}{prf} \quad [\text{m}] \tag{2.8}$$

$T_s$ is the echo signal sample time and *prf* is the Radar pulse repetition frequency.

In the horizontal plane the range dimension of a resolution cell and the range pixel spacing must be divided by the factor:

$$f_h = sin(a) \tag{2.9}$$

where $a$ is the incidence angle of the electromagnetic wave in the scene.

If two images have different values of $T_S$, $v$, *prf* or $a$, they have different pixel spacings, and therefore different scale factors. Consequently, they can not be registered only with a shift operation. In the interferometry process, the same scene is observed from different positions, therefore the images are observed with different incidence angles $a$ and then even though they have the same parameter $T_S$, the images have different range scales.

For images with different values of $T_p$, $q_a$, $\gamma$, $v$, $\lambda$ or $a$, the resolution cells of the two images are different and the resolution cells can not have a perfect superposition, therefore two registered pixels show a statistical decorrelation. FIG. 2.1

As an example, **Figure 2.1** shows a cut in range and azimuth of two simulated ERS-1 SAR images with point targets. Image 1: $T_S$ = 52.72 ns (pixel space in range: 7.91m) , *prf* = 1634.55 Hz (pixel spacing in azimuth: 4.34m) and sensor altitude equal to 800.0 km. Image 2: $T_S$ = 66.07 ns (pixel spacing in range: 9.91m), *prf* = 1934.55 Hz (pixel spacing in azimuth: 3.67m) and sensor altitude equal to 800.2 km. The baseline between the SAR sensors is 538.52 m and the baseline inclination is 21.80°. The images have different scale factors and therefore the point targets are not registered.

**II Jornada Latino-Americana de Sensoriamento Remoto por Radar: Técnicas de Processamento de Imagens**
**Santos, 11-12 de setembro de 1998**

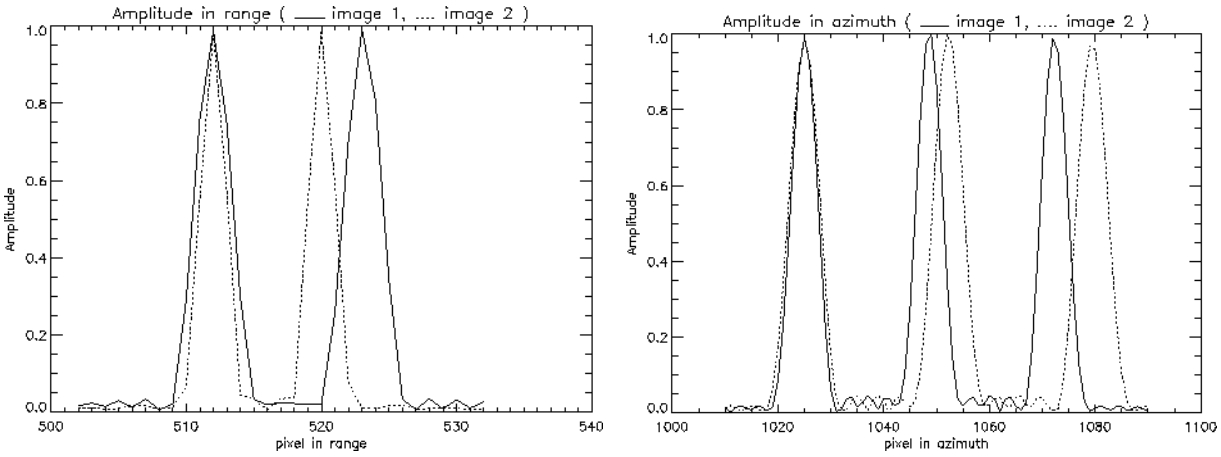


Figure 2.1: simulated point targets images with different scale factors.

A sample of a Synthetic Aperture Radar image, *s(r,x)*, can be represented approximately by:

$$s(r,x) = \iint h_r(r-r', x-x'; r').\, g(r', x') \exp\left\{-\frac{4.p}{l} r'\right\} dx'.dr' \tag{2.10}$$

where: $r$ and $x$ are, respectively, the radial and azimuth dimensions, $g(r', x')$ is the scene complex reflectivity at $(r', x')$, $h_r(.,.;.)$ is the SAR Point Spread Function, range dependent, and $\exp\left\{-\frac{4p}{l} r'\right\}$ is the phase due the round trip delay between the radar and the scatterers. The complex reflectivity $g(r,x)$ is a function of the backscattering coefficient $s_o$:

$$| g(r,x) |^2 = s_o(r,x) \tag{2.11}$$

An ideal point target at $(r_o, x_o)$, can be represented by a Dirac Function:

$$g(r,x) = c\ \ d(r-r_o, x-x_o) \tag{2.12}$$

where $c$ is a complex constant and $\delta(.,.)$ is the Dirac Function.

In this case, the SAR image is the Point Spread Function:

$$s(r,x) = c\ h_r(r-r_o, x-x_o; r_o) \exp\left\{-\frac{4.p}{l} r_o\right\} \tag{2.13}$$

If the SAR is ideal, its Point Spread Function is the Dirac Function:

$$h_r(r,x) = k\ \ d(r,x) \tag{2.14}$$

where $k$ is a complex constant.

For this function, the SAR image is the complex reflectivity of the scene:

$$s(r,x) = k\ \ g(r,x) \exp\left\{-\frac{4.p}{l} r\right\} \tag{2.15}$$

For a SAR sensor, the Punctual Spread Function can be approached by, Carrara et al. (1995):

$$h_r(r,x) = k\,\frac{\mathrm{sen}(p.x/D_a)}{p.x/D_a}\,\frac{\mathrm{sen}(p.r/D_r)}{p.r/D_r} \tag{2.16}$$

## 3 Range and azimuth scaling

We will suppose that we have two SAR images to be registered. One of them is the reference image and the other will be registered with the former. We will also suppose that the central pixel of both images are registered and that the scale factor to be applied in azimuth and range in the second image to be registered are, respectively, $F_a$ and $F_r$. If the reference image is represented by $s_{ref}(t,t)$ the second registered image will be $s(t.F_r, t/F_a)$. The relationship between $(t,t)$ and *(r,x)* used in Section 2 is given by:

$$(t,\ t) = \left(\frac{2}{c_o}r,\ \frac{1}{v}x\right)$$

We will assume that the second image raw data is represented by $pp(t,t)$ in the range time ($\tau$) and azimuth time (t) domain.

### 3.1 Azimuth scaling

We will consider a point target at $(t_o, t_o)$, whose raw data due the second SAR sensor is represented by:

$$\begin{aligned} pp(t,t;t_o,t_o) = a(t).s(t-2.R(t;r_o,t_o)/c_o).\exp\{-jp\,g(t-2.R(t;r_o,t_o)/c_o)^2\} \\ \times\ \exp\{-j4pR(t;r_o,t_o)/\,l\} \end{aligned} \tag{3.1}$$

with,

$$r_o = \frac{c_o}{2}t_o \tag{3.2}$$

$$R(t;r_o,t_o) = \sqrt{r_o^2 + v_2^2(t-t_o)^2} \tag{3.3}$$

where: a(.) is the antenna azimuth function, s(.) is the transmitted pulse amplitude, $\exp\{-p\,g^2\}$ is the range chirp and $\exp\{-j4p\sqrt{r_o^2+v_2^2(t-t_o)^2}\,/\,l\}$ is the azimuth phase modulation, $v_2$ is the relative velocity between the scatter and the second sensor platform and $t_o = 0$ is the scene azimuth center.

The azimuth scaling can be modified multiplying the raw data $pp(t,t;t_o,t_o)$ by:

$$f_0(t;r_o) = \exp\{-jp(F_a-1)\,g_a\,t^2\} \tag{3.4}$$

with the azimuth scaling $F_a$ given by:

$$F_a = \frac{v_1\ prf_2}{v_2\ prf_1} \tag{3.5}$$

where, $prf_1$ is the pulse repetition frequency of the reference SAR sensor, $v_1$ is the relative velocity between the scatter and the reference sensor platform, $prf_2$ is the pulse repetition

frequency of the SAR which generated the raw data of the secondary image, and $g_a$ is the azimuth chirp rate:

$$g_a = \frac{2.v_2^2}{l.r_o} \tag{3.6}$$

After the multiplication: $pp(t,t;t_o,t_o).f_o(t;r_o)$, the resulting signal has a new azimuth modulation term with azimuth phase center at $t_o / F_a$ instead $t_o$, Fernandes et al. (1996):

$$\exp\left\{- j4p\sqrt{r_o^2 + F_a v_2^2 (t - t_o / F_a)^2}\right\},$$

and a new azimuth chirp rate given by:

$$g_{a\,\mathrm{mod}} = g_a F_a \tag{3.7}$$

With this new phase center and after the azimuth focus we obtain the azimuth scaling in the second SAR image.

### 3.2 Range scaling

The Chirp Scaling Algorithm, Raney et al. (1994), provides means to scale the SAR image, Moreira et al. (1996) and Fernandes et al. (1996).

The Fast Fourier Transform (FFT) applied in the azimuth direction of the SAR raw data, $pp(t,t)$, transforms the range time - azimuth time domain into the range time - azimuth Doppler domain.

$$pP(t, f) = FFT_{az}\{pp(t,t)\} \tag{3.8}$$

where $pP(t, f)$ is the raw data in the range time ($\tau$) and azimuth Doppler (f) domain.

The range cell migration trajectory in the $pP(t, f)$ image is given by, Raney et al. (1994):

$$R_f(f;r) = r + r\,C_s(f) \tag{3.9}$$

where $C_s(f)$ is the curvature factor:

$$C_s(f) = \frac{1}{\sqrt{1 - \left(\frac{l.f}{2.v}\right)^2}} - 1 \tag{3.10}$$

and *v* is the relative velocity between the scatter and sensor platform.

Equation (3.9) shows that the range cell migration at range *r* has a curvature given by $r\,C_s(f)$. This curvature is range dependent. To transform the range cell migration trajectory into a range independent trajectory, the $pP(t, f)$ image is multiplied by the chirp scaling phase given by, Raney et al. (1994):

$$f_1(t, f; r_{ref}) = \exp\left\{- j.p.K_s(f;r_{ref}).C_s(f)\left[t - t_{ref}(f)\right]^2\right\} \tag{3.11}$$

where: $r_{ref}$ is the reference range, it will be choosen in the center of the scene, and $K_s(f;r_{ref})$ is a function of $f$ with $r_{ref}$ as a parameter.

$$t = \frac{2.r}{c_o} \tag{3.12}$$

and

$$t_{ref}(f) = \frac{2}{c_o} r_{ref} \left[1 + C_s(f)\right] \tag{3.13}$$

After the multiplication: $pP(t, f).f_1(t, f; r_{ref})$, the resulting image has a range cell migration trajectory given by:

$$R_f(f; r) = r + r_{ref}\ C_s(f) \tag{3.14}$$

The equation (3.14) shows that the range cell migration at range *r* has a curvature given by $r_{ref}\ C_s(f)$. This curvature is range independent.

The property of the chirp scaling phase to equalize the range cell migration can be extended to provide a scale in range, Moreira et al. (1996) and Fernandes et al. (1996).

For a range scaling factor of $F_r$, it must be choosen for the chirp scaling phase $f_1(t, f; r_{ref})$ a new curvature factor (the modified curvature factor) given by:

$$C_{scl}(f) = C_s(f) + (1 - F_r)\frac{1 + C_s(f)}{F_r} \tag{3.15}$$

If the scale factor is one, there is no scaling. This scaling is given by, Fernandes (1996):

$$F_r = \frac{T_{s2}.sin(a_2)}{T_{s1}.sin(a_1)} \tag{3.16}$$

where $a_1$ and $a_2$ are, respectively, the incidence angle in the center of the scene observed by the reference SAR sensor and the secondary SAR sensor. $T_{s1}$ and $T_{s2}$ are, respectively, the echo signal sample time of the reference and secondary SAR sensors.

With this new factor, the range cell migration will be equalized and scaled. The new range cell migration trajectory will be given by:

$$R_f(f; r) = r_{ref} + (r - r_{ref})\ F_r + r_{ref}\ C_s(f) \tag{3.17}$$

In (3.17) we note that the curvature is constant and given by $r_{ref}\ C_s(f)$, the range *r* of (3.14) becomes $r_{ref} + (r - r_{ref})\ F_r$. This is equivalent to an expansion or contraction around the center point $r_{ref}$. For instance, if *r* is a set of distances: [10, 20, 30, 40, *50*, 60, 70, 80] with $r_{ref} = 50$ and $F_r = 0.9$, we will have the new set of distances around $r_{ref} = 50$: [14, 23, 32, 41, *50*, 59, 68, 77].

If we suppose that the central pixel of this image is registered with the central pixel of another image (reference image), both images can be registered by the range focus.

The modified curvature factor introduces in the chirp scaling algorithm a phase error that can be compensated, Moreira et al. (1996), Fernandes et al. (1996).

## 3.3 The modified chirp scaling algorithm

The modified version of the chirp scaling algorithm takes into account the modification introduced in the previous sections. Another method for the azimuth scaling and a new configuration for the modified chirp scaling algorithm (the extended chirp scaling algorithm) is given by Moreira et al. (1996).

FIG. 2.1

**Figure 3.1** shows the point targets of **Figure 2.1** registered in range and azimuth by the proposed modified version of the chirp scaling algorithm.

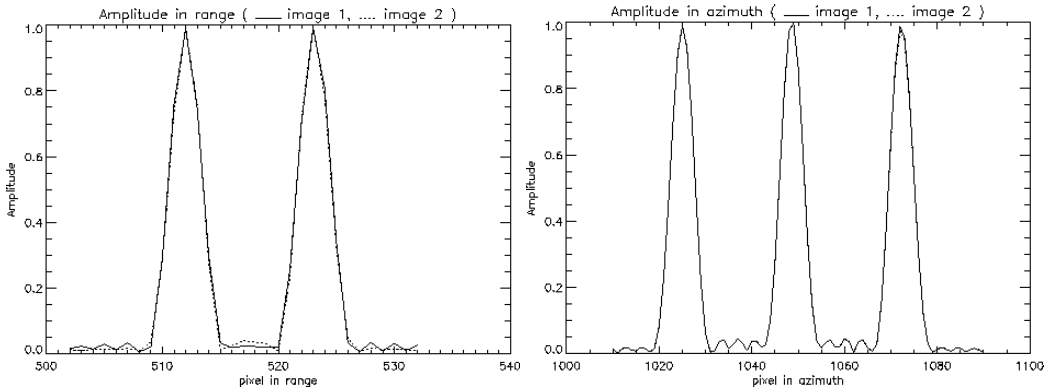


Figure 3.1: registered points targets.

The chirp scaling and the modified chirp scaling block diagram are shown respectively in **Figure 3.2.a** and **3.2.b**, Raney et al. (1994), Fernandes et al. (1996).

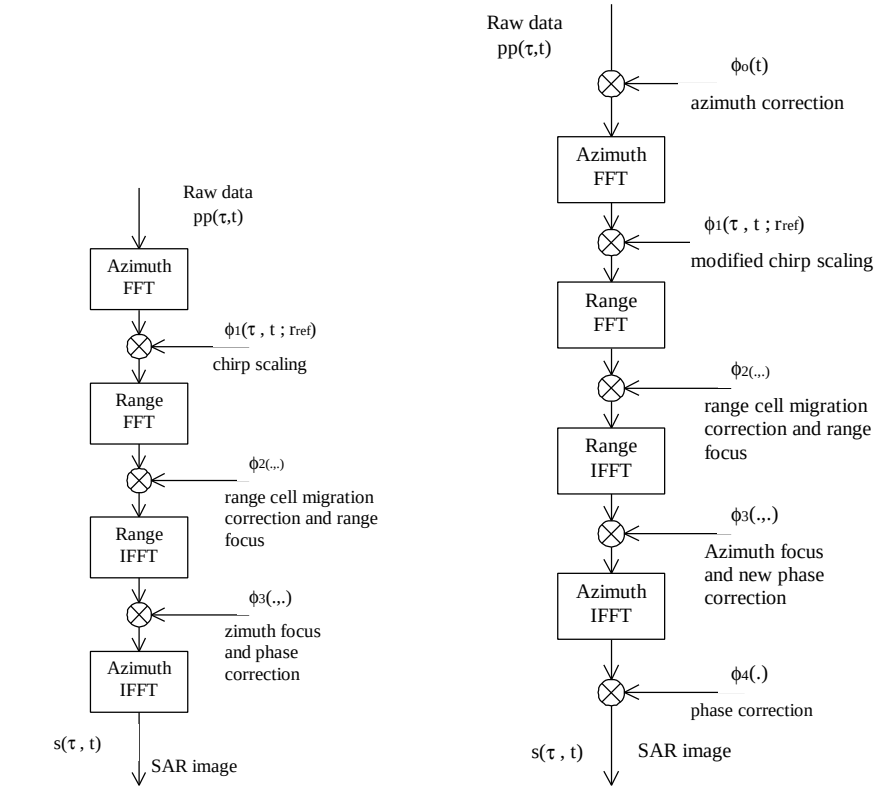


a) chirp scaling b) modified chirp scaling

Figure 3.2: chirp scaling algorithm.

## 4 Interferometric processor

Using the scaling in range and azimuth discussed in the previous section, it was developed an interferometric processor. This processor simultaneously generates and registers two SLC SAR images, calculates the interferogram, the fringes with flat earth correction and the coherence map. The processor input are two sets of SAR raw data, the satellites orbits, velocities and the radar and signal parameters. **Figure 4.1** shows the interferometric processor general block diagram.

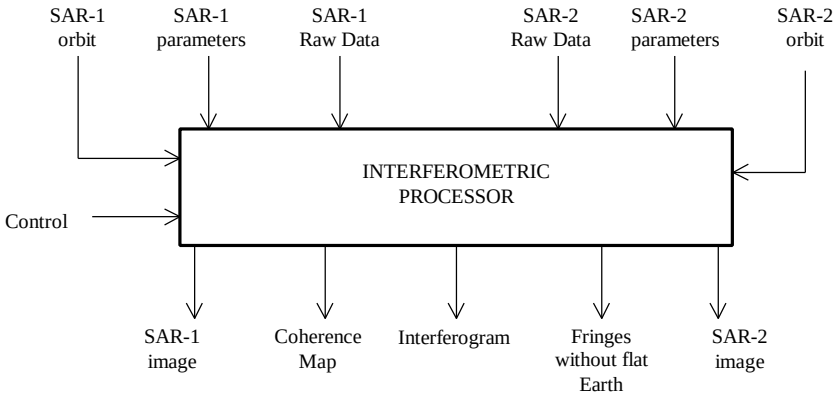


Figure 4.1: input/output of the interferometric processor

As an example, **Figure 4.2** shows the interferogram and the fringes, with flat Earth correction, from two registered images obtained from the ERS-1 SAR sensor over Fayoum-Rayan area (35Km in range, 32 Km in azimuth) near Cairo City.

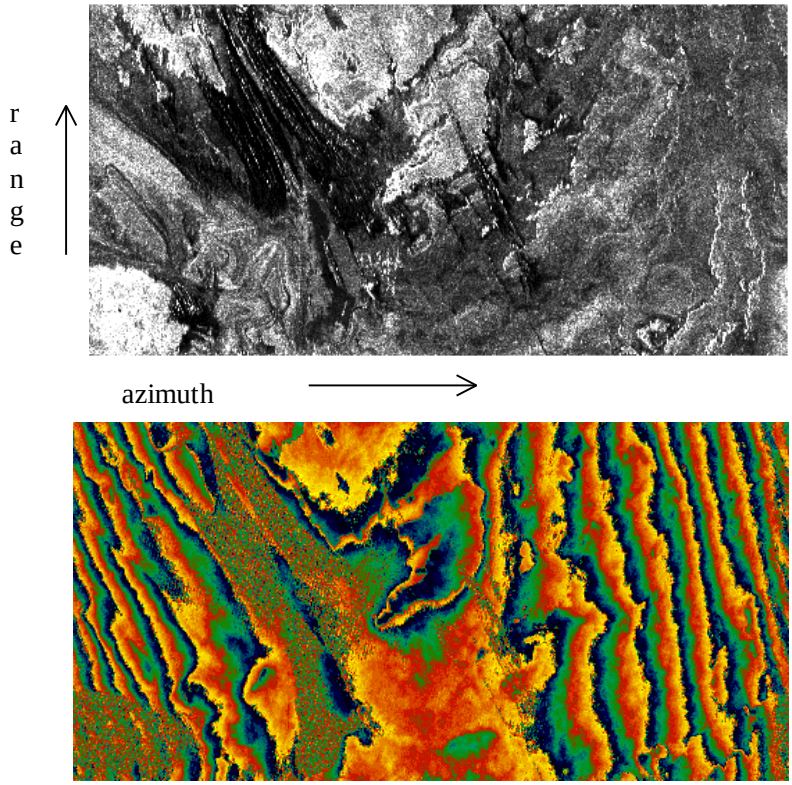


Figure 4.2: interferogram and fringes, with flat earth correction.

The processor selects one image as a reference image. The reference image is generated and the secondary image are simultaneously generated and registered with the former. If the SAR raw data are very big the processor divide the raw data in a small sets of data (2kB x 2kB or 4kB x 4kB blocks of data) and processes each set of data. The **Figure 4.3** shows the block diagram of the interferometric processor for each set of raw data.

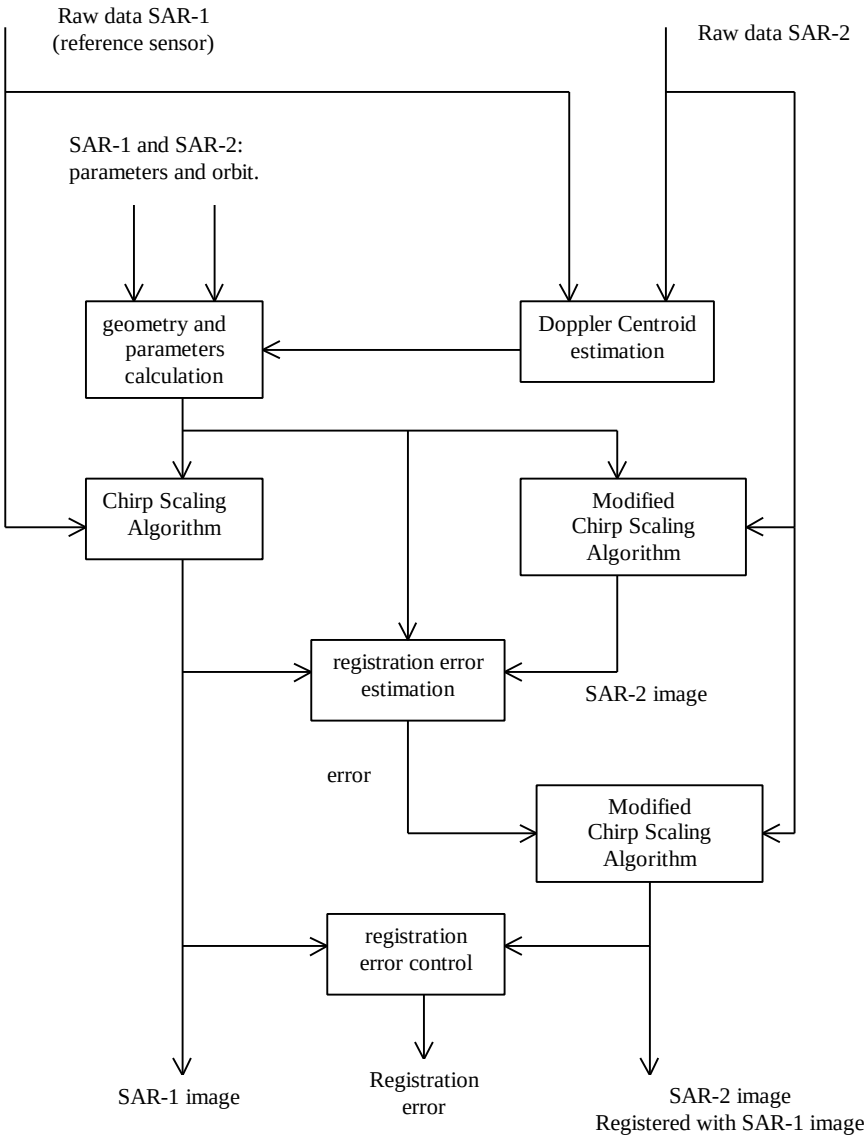


FIG. 4.4

Figure 4.3: registration process.

**Figure 4.4** shows the calculation of the interferogram, fringes and coherence map for two registered SLC SAR images, Mura (1993), Alenn, (1995). FIG. 4.5

As an example, **Figure 4.5** shows a ERS-1 amplitude image of a pair of images and the coherence map of these images from Düsseldorf area in Germany.

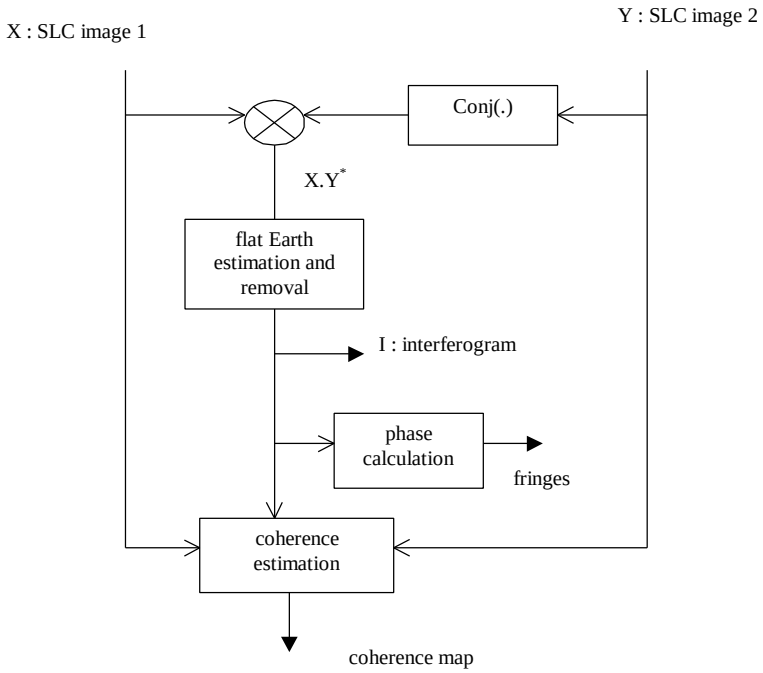


Figure 4.4: interferogram, fringes and coherence map calculation.

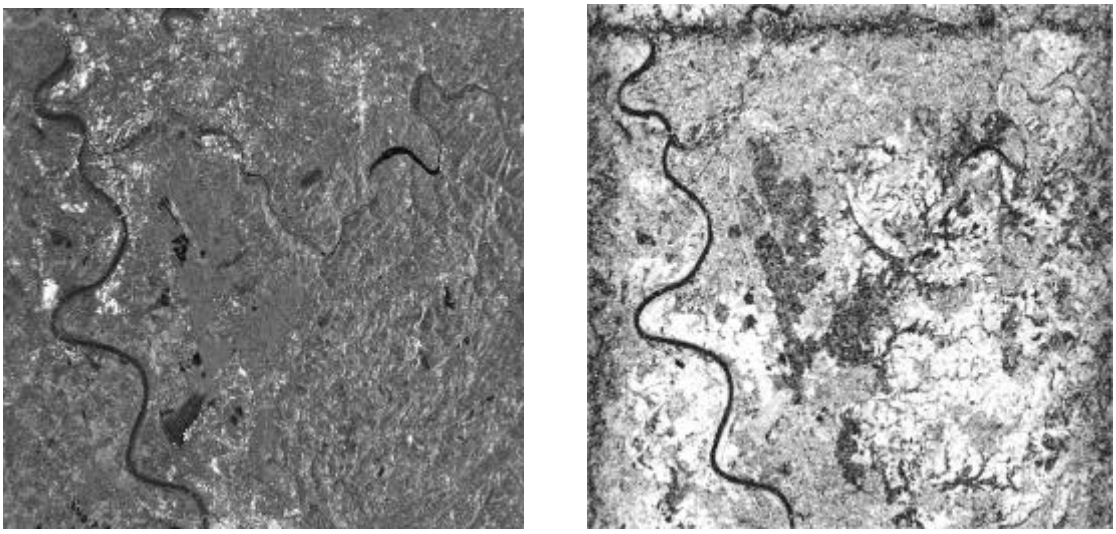

a) amplitude image b) coherence map

Figure 4.5: a ERS amplitude image and the coherence map of two ERS-1 images from Düsseldorf area in Germany, Reigber (1997).

## 5 Conclusions

The proposed procedure combines the SAR images generation and registration. The integrated processes reduces the computing time and preserve the image quality. The developed procedure was used in a interferometric processor that calculates the interferogram, the fringes and the coherence map.

The performance of the processor has been tested by the registration of simulated point targets and by the interferometric processing of real ERS-1 raw data.

## Acknowledgments

The author wish to tanks the Institut für Hochfrequenztechnik (HF) - Deutsches Zentrum für Luft- und Raumfahrt (DLR) in Oberpfaffenhofen/Germany, the International Civil Aviation Organizaton (ICAO) Project BRA-95/802 Objective 6-ITA and the Fundação de Amparo à Pesquisa do Estado de São Paulo (FAPESP) for their support in this work.

## References

Allen, C. *Interferometry Synthetic Aperture Radar*. IEEE Geoscience and Remote Sensing Society Newsletter, Sept., 1995, pp. 6-13.

Carrara, W.; Goodman, R. S.; Majewski, M. *Spotlight Synthetic Aperture Radar: signal processing algorithms*. Artech House, Boston, 1995.

Fernandes, D.; Waller, G. Moreira, J. R. Registration of SAR images using the chirp scaling algorithm, International Geoscience and Remote Sensing Symposium *(IGARSS'96)*, Nebrasca, 1996, *Proceedings*, pp. 799-801.

Fornaro, G.; Franceschetti, G.; Marzouk, E. S. A new approach for image registration in interferometric processing. . *Proceedings, International Geoscience and Remote Sensing Symposium (IGARSS`94)*, Seatle, 1998, pp. 1983-1985.

Moreira, A.; Scheiber, R.; Mittermayer, J. Extended Chirp Scaling Algorithm for Air- and spaceborne SAR data processing Stripmap and ScanSAR. *IEEE Transactions on Geoscience and Remote Sensing*, V. 34, No. 5, pp. 1123-1136, September, 1996.

Mura, J. C. Performance and interferometric capabilities of the INPE/DLR SAR processor. Deutsche gesellschaft für Ortung und Navigation e. v. 8, Radarsymposium, sept., 1993, pp. 166-171.

Reigber, A. Multitemporale Analyse der Kohärenz von SAR-Daten. *Diplomarbeit*, Universität Konstanz / Institut für Hochfrequenztechnik (HF) der Deutsches Zentrum für Luft- und Raumfahrt (DLR), 1997.

Raney, R. K.; Runge, H.; Bamler, R.; Cumming, I. G.; Wong, F. H. Precision SAR processing using chirp scaling. *IEEE Transactions on Geoscience and Remote Sensing*, V. 32, No. 4, 1994, pp. 786-799.